The Astrophysical Journal Letters, 841:L25 (6pp), 2017 June 1 https://doi.org/10.3847/2041-8213/aa7338

Rotating Starburst Cores in Massive Galaxies at $z = 2.5$

Ken-ichi Tadaki[1,2], Tadayuki Kodama[2,3], Erica J. Nelson[1], Sirio Belli[1], Natascha M. Förster Schreiber[1], Reinhard Genzel[1,4,5], Masao Hayashi[2], Rodrigo Herrera-Camus[1], Yusei Koyama[6], Philipp Lang[7], Dieter Lutz[1], Rhythm Shimakawa[3], Linda J. Tacconi[1], Hannah Übler[1], Emily Wisnioski[1], Stijn Wuyts[8], Bunyo Hatsukade[9], Magdalena Lippa[1], Kouichiro Nakanishi[2,3], Soh Ikarashi[10], Kotaro Kohno[9,11], Tomoko L. Suzuki[3], Yoichi Tamura[9], and Ichi Tanaka[6]

[1] Max-Planck-Institut für extraterrestrische Physik, Giessenbachstrasse, D-85748 Garching, Germany
[2] National Astronomical Observatory of Japan, 2-21-1 Osawa, Mitaka, Tokyo 181-8588, Japan; tadaki.ken@nao.ac.jp
[3] Department of Astronomical Science, SOKENDAI (The Graduate University for Advanced Studies), Mitaka, Tokyo 181-8588, Japan
[4] Department of Physics, Le Conte Hall, University of California, Berkeley, CA 94720, USA
[5] Department of Astronomy, Hearst Field Annex, University of California, Berkeley, CA 94720, USA
[6] Subaru Telescope, National Astronomical Observatory of Japan, 650 North A'ohoku Place, Hilo, HI 96720, USA
[7] Max-Planck-Institut für Astronomie, Königstuhl 17, D-69117 Heidelberg, Germany
[8] Department of Physics, University of Bath, Claverton Down, Bath BA2 7AY, UK
[9] Institute of Astronomy, The University of Tokyo, 2-21-1 Osawa, Mitaka, Tokyo 181-0015, Japan
[10] Kapteyn Astronomical Institute, University of Groningen, P.O. Box 800, 9700AV Groningen, The Netherlands
[11] Research Center for the Early Universe, The University of Tokyo, 7-3-1 Hongo, Bunkyo, Tokyo 113-0033, Japan
Received 2017 March 29; revised 2017 May 10; accepted 2017 May 14; published 2017 May 26

Abstract

We present spatially resolved ALMA observations of the CO $J = 3 - 2$ emission line in two massive galaxies at $z = 2.5$ on the star-forming main sequence. Both galaxies have compact dusty star-forming cores with effective radii of $R_e = 1.3 \pm 0.1$ kpc and $R_e = 1.2 \pm 0.1$ kpc in the 870 μm continuum emission. The spatial extent of star-forming molecular gas is also compact with $R_e = 1.9 \pm 0.4$ kpc and $R_e = 2.3 \pm 0.4$ kpc, but more extended than the dust emission. Interpreting the observed position–velocity diagrams with dynamical models, we find the starburst cores to be rotation dominated with the ratio of the maximum rotation velocity to the local velocity dispersion of $v_{max}/\sigma_0 = 7.0^{+2.5}_{-2.8}$ ($v_{max} = 386^{+36}_{-32}$ km s^{-1}) and $v_{max}/\sigma_0 = 4.1^{+1.7}_{-1.5}$ ($v_{max} = 391^{+54}_{-41}$ km s^{-1}). Given that the descendants of these massive galaxies in the local universe are likely ellipticals with v/σ nearly an order of magnitude lower, the rapidly rotating galaxies would lose significant net angular momentum in the intervening time. The comparisons among dynamical, stellar, gas, and dust mass suggest that the starburst CO-to-H_2 conversion factor of $\alpha_{CO} = 0.8\,M_\odot\,(\mathrm{K\,km\,s^{-1}\,pc^{-2}})^{-1}$ is appropriate in the spatially resolved cores. The dense cores are likely to be formed in extreme environments similar to the central regions of local ultraluminous infrared galaxies. Our work also demonstrates that a combination of medium-resolution CO and high-resolution dust continuum observations is a powerful tool for characterizing the dynamical state of molecular gas in distant galaxies.

Key words: galaxies: evolution – galaxies: high-redshift – galaxies: ISM

1. Introduction

Massive quiescent galaxies often have dense cores (Fang et al. 2013; van Dokkum et al. 2014) while the morphology of star-forming galaxies is typically dominated by exponential disks rather than central bulges (e.g., Wuyts et al. 2011b). Massive star-forming galaxies are expected to transform their morphology from disk dominated to bulge dominated. Understanding the formation history of the bulge component is a critical step toward revealing the origin of the Hubble sequence. At the peak epoch of galaxy formation ($z \sim 2$), the most massive, $\log(M_*/M_\odot) > 11$, star-forming galaxies still have extended disks, but are rapidly building up their central cores through dusty, compact starbursts (Barro et al. 2016; Tadaki et al. 2017). Bulge formation in a short period of <1 Gyr at $z \sim 2$ is also corroborated by observations of old stellar populations and enhanced [α/Fe] ratios in massive quiescent galaxies at $z \sim 1$ (e.g., Belli et al. 2015; Onodera et al. 2015). All these findings suggest that central cores of massive galaxies have a different formation history than outer disks. The next step is to characterize the kinematics of these dense cores in the process of formation, which will shed light on their formation mechanisms and subsequent evolution.

At high redshift, the kinematics of dusty star-forming cores in massive galaxies are difficult to study. While Hα studies with near-infrared spectrographs have made significant progress in understanding the kinematics of core formation (e.g., Barro et al. 2014; Nelson et al. 2014; E. Wisnioski et al. 2017, in preparation), the Hα line is not an ideal tool for investigating the kinematics of forming cores because of dust attenuation. Multi-wavelength high-resolution imaging and emission line maps reveal that the central regions in massive high-redshift galaxies are often strongly attenuated by dust (Nelson et al. 2016; Tacchella et al. 2017). CO line observations provide a more robust means of obtaining kinematic information for dusty objects, as well as the molecular gas properties (e.g., Tacconi et al. 2008; Ivison et al. 2013).

In local ultraluminous infrared galaxies (ULIRGs), molecular gas is concentrated into rotating nuclear disks or rings (e.g., Downes & Solomon 1998). The physical condition of the gas is totally different from that in normal star-forming galaxies. In normal star-forming regions, CO emission mainly comes from an ensemble of self-gravitating molecular clouds. Although the CO line is typically optically thick in each virialized molecular cloud, it is possible to count the number of clouds and estimate the total molecular gas mass. We use the

CO-to-H_2 conversion factor of $\alpha_{CO} = M_{gas}/L'_{CO} = 4.36\,M_\odot$ $(K\,km\,s^{-1}\,pc^{-2})^{-1}$ including a correction for helium since it is calibrated by virial mass measurements, optically thin dust emission, and γ-ray observations in the Milky Way disk (see the review in Bolatto et al. 2013).

A CO-based gas mass with the Galactic conversion factor, however, often equals or exceeds a dynamical mass in local ULIRGs and SMGs, which could imply a smaller conversion factor (e.g., Downes & Solomon 1998; Tacconi et al. 2008). This variation of α_{CO} could be caused by a high star formation rate (SFR) surface density in extreme environments. The intense UV radiation heats the nearby dust, and the gas temperature increases through efficient energy exchange with hot dust (Narayanan et al. 2012). Then, the CO surface brightness increases more rapidly than the gas mass surface density.

In this Letter, we report results from CO $J = 3 - 2$ observations of two massive galaxies at $z = 2.5$ using the Atacama Large Millimeter/submillimeter Array (ALMA) to study the spatial distribution and the kinematics of molecular gas in the starburst cores. We assume a Chabrier initial mass function (Chabrier 2003) and adopt cosmological parameters of $H_0 = 70\,km\,s^{-1}\,Mpc^{-1}$, $\Omega_M = 0.3$, and $\Omega_\Lambda = 0.7$.

2. Observations

We focus on the most massive star-forming galaxies with $\log(M_*/M_\odot) > 11$ since this mass range is important for formation of dense cores (e.g., Tadaki et al. 2017). We select two galaxies at $z = 2.53$ (U4-16795 and U4-16504) from Subaru narrowband imaging in the SXDF field (Tadaki et al. 2013). The narrowband-based redshift has uncertainties of $\Delta z \pm 0.02$. The two galaxies are located within the primary beam of ALMA Band-3 receivers (a beam width at half power of $\sim 1'$) as the projected separation is $9\farcs7$. Both galaxies have a compact dusty star-forming core, which is probed by 870 μm dust continuum emission (Tadaki et al. 2017). We compute the stellar mass using the FAST spectral energy distribution fitting code (Kriek et al. 2009) and the 3D-*HST* multi-wavelength photometric catalog (Skelton et al. 2014) using the stellar population synthesis models of Bruzual & Charlot (2003), exponentially declining star formation histories and the dust attenuation law of Calzetti et al. (2000). The total stellar mass is $\log(M_*/M_\odot) = 11.26 \pm 0.15$ for U4-16795 and $\log(M_*/M_\odot) = 11.25 \pm 0.15$ for U4-16504. In deep HAWK-I/K_s-band maps (Fontana et al. 2014), 81% and 71% of the total fluxes come from the central $1\farcs5$ aperture region for U4-16795 and U4-16504, respectively. We take into account these factors when comparing the stellar mass with other masses (Section 4.2).

U4-16795 is detected in a deep *Herschel*-PACS 160 μm map from archival data (see Lutz et al. 2011 for the methodology) and U4-16504 is detected in a deep *Spitzer*-MIPS 24 μm map (PI: J. Dunlop). Following the recipes of Wuyts et al. (2011a), we derive SFRs of $\log(SFR/M_\odot\,yr^{-1}) = 2.62 \pm 0.1$ for U4-16795 and $\log(SFR/M_\odot\,yr^{-1}) = 2.37 \pm 0.25$ for U4-16504 from a combination of the rest-frame 2800 Å and infrared luminosities. The targets are located on the massive end of the star-forming main sequence at $z \sim 2$ (e.g., Speagle et al. 2014).

We observe the CO $J = 3 - 2$ emission line ($\nu_{rest} = 345.796$ GHz) of the two massive galaxies with ALMA Band-3 receivers covering the frequency range of 95–99 and 107–111 GHz. The calibration is processed through the Common Astronomy Software Application package (CASA; McMullin et al. 2007). We use the tclean task with natural weighting to make a channel map with a velocity width of $50\,km\,s^{-1}$ and dirty continuum maps excluding the frequency range of the CO line. The synthesized beamsize is $0\farcs66 \times 0\farcs55$. The rms levels are 147 μJy beam^{-1} in the channel map and 8.1 μJy beam^{-1} in the continuum map.

3. Results and Analysis

We robustly detect CO $J = 3 - 2$ emission in both galaxies as seen in the spatially averaged spectra within a $1\farcs5$ aperture (Figure 1). We measure total fluxes within a $1\farcs5$ aperture in the velocity-integrated maps to derive the CO line luminosities (Table 1). Both galaxies show a spatial offset between the blueshifted and redshifted CO components with a velocity width of $150\,km\,s^{-1}$ (Figure 1). The two central positions determine the kinematic major axis of the molecular gas disks. We also derive line-of-sight velocities by fitting a Gaussian function to the CO line spectrum in each spatial pixel. The velocity field maps show a monotonic gradient along the kinematic major axis (Figure 1), suggesting rotation of the molecular gas. In this section, we construct the dynamical model of the dusty star-forming cores through the following three steps: (1) determining a minor-to-major axis ratio ($q = b/a$) of the 870 μm continuum emission, (2) measuring an effective radius (R_e) of the CO line emission, and (3) exploring the best-fit dynamical model.

3.1. Spatial Extent of Dust

$0\farcs2$-resolution 870 μm continuum maps are available for both galaxies (Tadaki et al. 2017). In SMGs at high-redshift, the dust emission is well described by an elliptical exponential disk (Hodge et al. 2016). We derive effective radii, R_e, along the major axis of the 870 μm continuum emission assuming an inclined disk with an exponential profile, while Tadaki et al. (2017) have adopted circular disk models ($q = 1$). We use the UVMULTIFIT tool to fit the visibility amplitudes to models in the u–v plane (Martí-Vidal et al. 2014). For U4-16795, the best-fit values and fitting errors are $R_e = 1.3 \pm 0.1$ kpc, $q = 0.49 \pm 0.07$ and the position angle is $PA_{mor} = 35° \pm 5°$. Note that the morphological major axis of the 870 μm continuum emission is well aligned with the kinematics major axis of the CO line emission ($|PA_{mor} - PA_{kin}| = 8°$), supporting ordered rotation (Wisnioski et al. 2015). We also perform the visibility fitting for U4-16504 with an elliptical disk, but could not obtain meaningful constraints on the axis ratio. Circular disk models give an effective radius of $R_e = 1.2 \pm 0.1$ kpc.

3.2. Spatial Extent of Molecular Gas

Next, we derive effective radii of the CO line emission using the axis ratio of the dust emission. We fix to $q = 0.49$ and $PA_{mor} = 35°$ for U4-16795 and $q = 1$ for U4-16504. Figure 2 shows the observed visibility amplitudes and the best-fit models. The effective radii are $R_e = 1.9 \pm 0.4$ kpc for U4-16795 and $R_e = 2.3 \pm 0.4$ kpc for U4-16504, which are larger than those of the 870 μm continuum emission. This result naively suggests that the dust is more concentrated than the molecular gas, which is consistent with negative radial gradients in the dust-to-gas mass ratio seen in nearby star-forming galaxies (Magrini et al. 2011). On the other hand, galaxy centers tend to have higher dust temperatures compared to the outer region (Galametz et al. 2012), making the dust mass size larger than the 870 μm

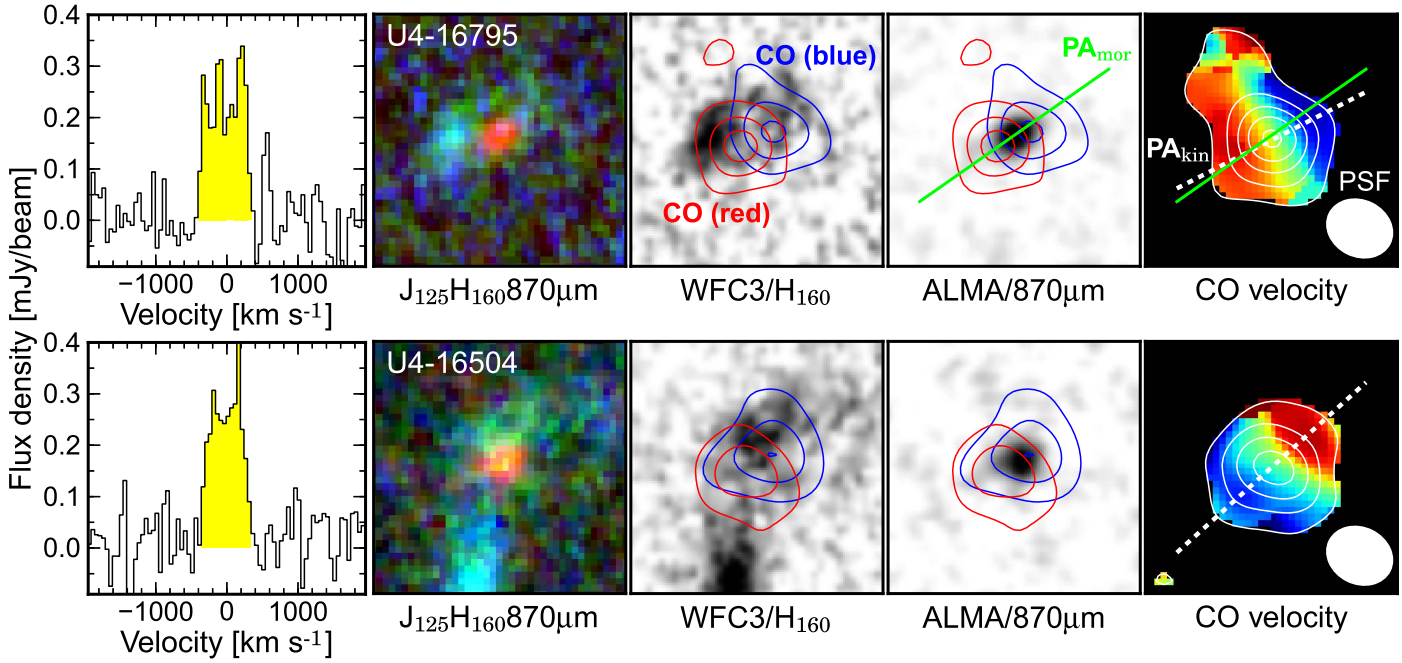

Figure 1. Two massive galaxies at $z = 2.5$ detected in the CO $J = 3 - 2$ line. From left to right: spatially averaged CO spectra; three-color images with *HST*/F125W-, F160W-, and ALMA/870 μm-band ($2\farcs5 \times 2\farcs5$), monochromatic images at F160W- and 870 μm-band with blue and red contours displaying blueshifted and redshifted CO components with a velocity width of 150 km s^{-1}; CO velocity field with white contours indicating the velocity-integrated CO fluxes. The contours are plotted every 3σ. Green and white dashed lines indicate the morphological major axis of 870 μm continuum emission and the kinematic major axis of CO, respectively.

size. High-resolution ALMA observations at a high-frequency band (e.g., 450 μm) will allow us to determine the radial gradient in dust temperature (Section 4.1) and identify if the apparent size difference originates in the dust properties or the intrinsic gradients of dust-to-gas mass ratio.

3.3. Molecular Gas Kinematics

We find that both massive galaxies observed here exhibit signatures of disk-like rotation in their CO velocity fields (Figure 1). Assuming that the molecular gas is in rotating disks, we investigate the kinematic properties by fitting dynamical models to the data in the position–velocity (PV) diagram along the kinematic major axis (Figure 3). We use the DYSMAL code (Davies et al. 2011) to generate PV diagrams for an exponential disk, spatially convolved with a $0\farcs66 \times 0\farcs55$ Gaussian beam. We take into account the effect of pressure support, reducing the observed rotation velocity (e.g., Burkert et al. 2010; Wuyts et al. 2016). The effective radii of the gas disks are fixed to those measured in Section 3.2. For U4-16795, we infer an inclination, i, from the axis ratio of the 870 μm dust continuum emission as $\sin^2 i = (1 - q^2)/(1 - \text{thickness}^2)$ for symmetric oblate disks with an intrinsic thickness of 0.25 (van der Wel et al. 2014). The inclination is $\log(1/\sin^2 i) = 1.11 \pm 0.04$ dex (corresponding to $i = 64°$). This uncertainty propagates to the dynamical mass estimate as $M_{\rm dyn} \propto 1/\sin^2 i$. As the effective radius and the inclination are fixed, the remaining free parameters in the model are dynamical mass, $M_{\rm dyn}$, and local velocity dispersion, σ_0. For U4-16504, we adopt the average of possible inclinations ($\langle \sin i \rangle = 0.79$) in the case of isotropically oriented disks (see the appendix of Law et al. 2009). As the standard deviation is derived as $(\int (\sin i - \langle \sin i \rangle)^2 \sin i \; di / \int \sin i \; di)^{1/2} = 0.22$, we adopt the uncertainty of $\Delta \log(1/\sin^2 i) = \pm 0.09$ dex.

In the PV diagrams, we use the pixels with a flux above 3σ to calculate the chi-squared values between the data and the models. Figure 3 shows the best-fit models to minimize the chi-squared value along with the residual maps after subtracting the model from the data. The best-fit models for the two galaxies have dynamical masses $\log(M_{\rm dyn}/M_\odot) = 11.10^{+0.07}_{-0.06}$ for U4-16795 and $\log(M_{\rm dyn}/M_\odot) = 11.19^{+0.12}_{-0.09}$ for U4-16504. These uncertainties are based on the reduced-chi-squared values corresponding to a p-value above 5%. In the dynamical mass measurements, after taking into account the uncertainties of effective radius and inclination, our final uncertainties are +0.13 dex (−0.12 dex) for U4-16795 and +0.17 dex (−0.15 dex) for U4-16504.

We also derive the rotation velocity and local velocity dispersion from the best-fit models. We find $v_{\rm max} = 386^{+36}_{-32}$ km s^{-1} and $\sigma_0 = 55^{+19}_{-22}$ for U4-16795 and $v_{\rm max} = 391^{+54}_{-41}$ km s^{-1} and $\sigma_0 = 96^{+35}_{-31}$ km s^{-1} for U4-16504. We note that they have a larger local velocity dispersion than the mean value ($\sigma_0 = 50$ km s^{-1}) in a large sample of rotation-dominated galaxies at $z \sim 2$ (Wisnioski et al. 2015). This means that both dusty star-forming cores are rotation dominated with the ratio of the maximum rotation velocity to local velocity dispersion of $v_{\rm max}/\sigma_0 = 7.0^{+2.5}_{-2.8}$ for U4-16795 and $4.1^{+1.7}_{-1.5}$ for U4-16504.

4. Dust and Gas Mass Estimates

4.1. Dust Mass

Rest-frame 850 μm continuum emission is a good indicator of dust mass, $M_{\rm dust}$. For galaxies at $z \sim 2$, rest-frame 850 μm (3 mm in the observed frame) fluxes are often extrapolated from ~1 mm fluxes using a modified blackbody radiation (MBB) model with a dust temperature of $T_d = 25$ K and the dust emissivity, $\kappa \propto \nu^\beta$, with an index of $\beta = 1.8$

Table 1
Galaxy Properties for Two Massive Star-forming Galaxies at $z = 2.5$

ID	z_{CO}	$S_{CO}dv$[a] (Jy km s^{-1})	$\log L'_{CO(3-2)}$ (K km s^{-1}pc^{-2})	$\log M_{dyn}$ ($M_\odot$)	$\log M_*$[b] ($M_\odot$)	$\log M_{gas,CO}$[b] ($M_\odot$) [$\alpha_{CO} = 4.36$]	$\log M_{gas,CO}$[b] ($M_\odot$) [$\alpha_{CO} = 0.8$]	$\log M_{gas,3mm}$[c] ($M_\odot$) [$\delta_{gdr} = 120$]
U4-16795	2.5236	0.72 ± 0.06	10.37 ± 0.04	$11.10^{+0.13}_{-0.12}$	11.17 ± 0.15	11.01 ± 0.04	10.28 ± 0.04	10.38–10.96
U4-16504	2.5267	0.72 ± 0.05	10.37 ± 0.03	$11.19^{+0.17}_{-0.15}$	11.10 ± 0.15	11.01 ± 0.03	10.27 ± 0.03	10.41–10.98

Notes.
[a] Velocity-integrated CO fluxes within the 1.″5 aperture. The uncertainties are estimated from the standard deviation of 200 random aperture photometry measurements.
[b] Stellar mass and CO-based gas mass within the 1.″5 aperture.
[c] The 5σ limit of 3 mm continuum-based gas mass within the 1.″5 aperture through the gas-to-dust ratio of 120. The range corresponds to the dust emissivity of $\kappa_{850} = 0.4$–1.5 g^{-1} cm^2.

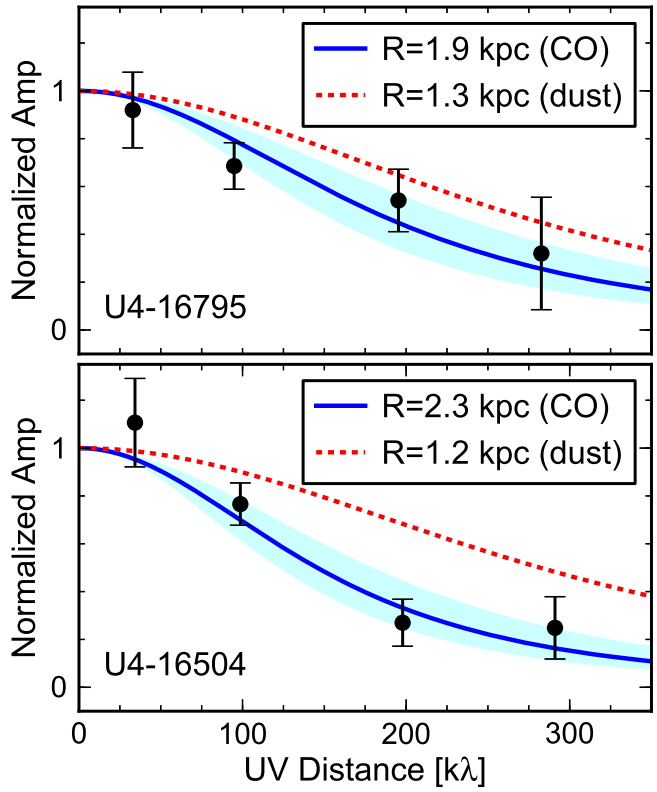

Figure 2. Visibility amplitudes of the velocity-integrated CO emission for U4-16795 (top) and U4-16504 (bottom). The blue solid line and the shaded region indicate the best-fitting model and the 1σ error, respectively. The red dashed line presents the best-fitting model of the 870 μm dust emission. The x-axis gives the circularized uv distance.

(e.g., Scoville et al. 2016) as

$$S_\nu = \frac{M_{\rm dust}\,\kappa_{\nu_{\rm rest}}\,B_{\nu_{\rm rest}}(T_{\rm d})(1+z)}{d_{\rm L}^2}, \quad (1)$$

where $d_{\rm L}$ is the luminosity distance. Making 870 μm maps with the same synthesized beam as the 3 mm maps, we measure peak fluxes of $S_{870\mu m} = 3.5 \pm 0.1$ mJy beam^{-1} for U4-16795 and $S_{870\mu m} = 2.2 \pm 0.1$ mJy beam^{-1} for U4-16504. They correspond to 77% and 78% of the total flux within a 1.″5 aperture. Although the MBB models give the extrapolated 3 mm fluxes of $S_{3mm} = 90 \pm 3$ μJy beam^{-1} for U4-16795 and $S_{3\,mm} = 55 \pm 3$ μJy beam^{-1} for U4-16504, we do not detect the 3 mm continuum emission above 5σ significance.

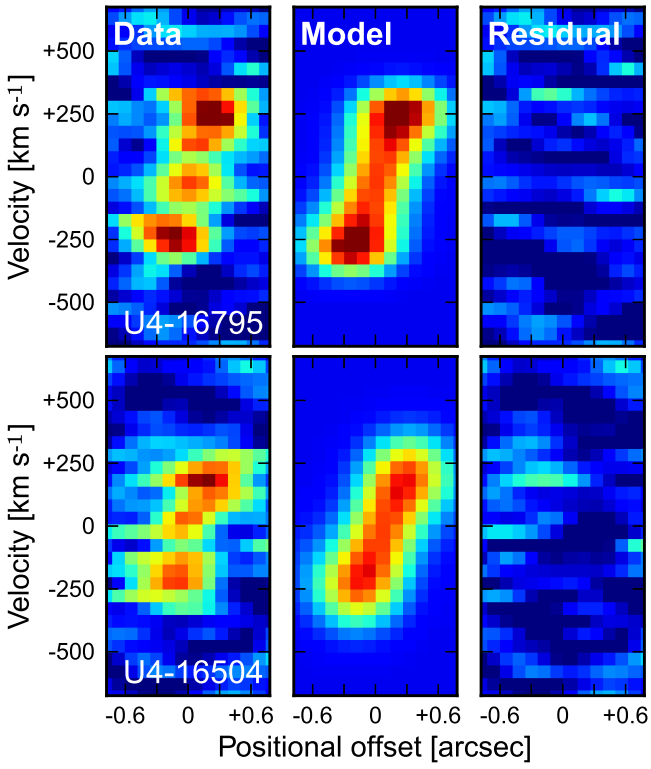

Figure 3. Observed position–velocity diagrams of the CO spectra (left). The middle and right panels show the best-fit dynamical model and the residuals between the data and the model, respectively.

Focusing on U4-16795, we evaluate the assumption of T_d and β. We also use the ALMA 1.1 mm flux ($S_{1.1mm} = 1.75 \pm 0.07$ mJy beam^{-1}; Tadaki et al. 2015). Figure 4 shows several MBB models with different dust temperatures and emissivity indices. The 5σ upper limit at 3 mm rejects the models with $T_d = 25$ K, suggesting a higher T_d or a steeper β. MBB models with an emissivity index in the usual range ($\beta = 1.5$–2.0; e.g., Dunne & Eales 2001) require a much higher dust temperature of $T_d > 60$ K to explain the faint 3 mm flux while they are inconsistent with the 160 μm flux. Therefore, we reasonably assume $T_d = 32$ K and $\beta = 2.2$ to explain all data points. In the range of the dust emissivity of $\kappa_{850} = 0.4$–1.5 g^{-1} cm^2 (Dunne et al. 2003), the 3-mm-based dust mass is $\log(M_{\rm dust,5\sigma}/M_\odot) = 8.30$–$8.88$ for U4-16795 and $\log(M_{\rm dust,5\sigma}/M_\odot) = 8.33$–$8.90$ for U4-16504. If we use the 870 μm flux assuming $T_d = 25$ K and $\beta = 1.8$, the estimated dust mass would become larger by 0.5 dex.

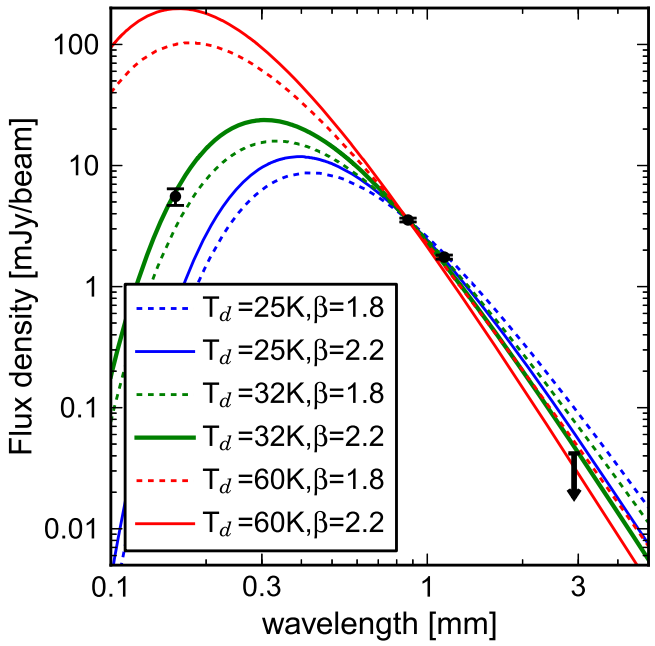

Figure 4. Dust continuum SED for U4-16795 with several types of modified blackbody radiation models. The black points are the fluxes measured at PACS 160 μm, ALMA 870 μm, and 1.1 mm. The upper limit is given by the 5σ flux at ALMA 3 mm.

4.2. Gas Mass

We estimate the CO-based gas masses using two conversion factors, $\alpha_{\rm CO} = 4.36\,M_\odot\,({\rm K\,km\,s^{-1}\,pc^{-2}})^{-1}$ (Galactic value) and $\alpha_{\rm CO} = 0.8\,M_\odot\,({\rm K\,km\,s^{-1}\,pc^{-2}})^{-1}$ (starburst value; Downes & Solomon 1998). We then compare the gas masses derived with these two different conversion factors to the dynamical and stellar masses. The CO $J = 3 - 2$ emission line is assumed to be thermalized (Bolatto et al. 2015). These mass measurements are summarized in Table 1. If we adopt the Galactic conversion factor, the baryonic mass fraction, defined as $f_{\rm bar} = (M_* + M_{\rm gas})/M_{\rm dyn}$, exceeds unity. Monte Carlo simulations incorporating the uncertainties of gas, stellar, and dynamical mass show that the probability of the baryonic mass fraction being less than one is 2.3% for U4-16795 and 17.1% for U4-16504. In the case of the starburst conversion factor, the probability is increased to 24.7% and 55.3%, respectively.

We also independently constrain the gas mass from the 3-mm-based dust mass, assuming a gas-to-dust ratio of 120 (Wilson et al. 2008). The 5σ upper limit is $\log(M_{\rm gas,5\sigma}/M_\odot) = 11$ (Table 1). The two independent approaches suggest that the starburst conversion factor is appropriate in the compact dusty star-forming region. Adopting the starburst conversion factor to derive the CO-based gas mass, we find the gas-to-dynamical mass fraction to be 15^{+4}_{-5}% for U4-16795 and 12^{+4}_{-5}% for U4-16504 and the gas depletion timescale to be $M_{\rm gas}/{\rm SFR} = 46 \pm 11$ Myr and 79 ± 46 Myr, respectively. When the uncertainties of the conversion factor are taken into consideration, those in the gas mass estimate become larger.

5. Discussion and Summary

Using ALMA observations of CO $J = 3 - 2$ emission, we find that the compact molecular gas in the star-forming cores of two massive galaxies is rapidly rotating. This has implications for both the formation and subsequent evolution of the cores of massive galaxies. The formation mechanism appears to be dissipative and the observed rotation indicates that at least some angular momentum is preserved in the star-forming molecular gas. Simulations show this could happen due to a gas-rich merger or disk instabilities (e.g., Wellons et al. 2015; Zolotov et al. 2015).

The two massive star-forming galaxies are both rotation dominated with $v/\sigma = 7.0^{+2.5}_{-2.8}$ and $v/\sigma = 4.1^{+1.7}_{-1.5}$. Kinematic studies of massive quiescent galaxies suggest they are rotating (Newman et al. 2015), although with lower v/σ than found here for their progenitors. Additionally, the descendants of these galaxies in the local universe are slow rotators with v/σ nearly an order of magnitude lower (Cappellari 2016), suggesting that the galaxies we observe need to lose significant net angular momentum in the intervening time. Our results support a picture in which net angular momentum is initially reduced during the quenching process and further during a growth phase by dry mergers.

We find that the molecular gas of the two massive galaxies at $z = 2.5$ is compact with $R_{\rm e} \sim 2$ kpc. Such a concentration of star-forming gas is consistent with a scenario in which a wet compaction events (radial transport of gas) could build the cores of massive galaxies (Zolotov et al. 2015). The two galaxies host even more compact starbursts with a high SFR surface density as traced by the dust continuum emission, rapidly building up dense cores and transforming the galaxy morphology from disk dominated to bulge dominated (Tadaki et al. 2017). If the gas mass in these galaxies is as low as our data suggest, we may be witnessing the end of the growth of these dense cores due to star formation.

Our independent measurements of dynamical, stellar, gas, and dust mass suggest that the starburst CO-to-H_2 conversion factor is appropriate for the spatially resolved cores. These dense cores are likely to be formed in extreme environments like central regions of local ULIRGs. The same conclusion is obtained by recent [C I] observations of a star-forming galaxy in the similar mass and redshift range (Popping et al. 2017) and CO observations of starburst galaxies above the main sequence (Sargent et al. 2014). On the other hand, it is not clear yet that the starburst conversion factor is appropriate for entire galaxies. Tacconi et al. (2017) investigated the variations in molecular gas properties for 650 galaxies over $0 < z < 3$ by compiling CO and dust continuum data and do not find the presence of such a large change in the conversion factor. A statistical study of the kinematics of the molecular gas is an essential next step for getting a consensus on this issue. However, high spatial resolution CO observations suffer from missing flux and are more time consuming compared to dust continuum observations. A combination of medium-resolution CO and high-resolution dust continuum observations is reasonable in terms of observing time and is a powerful tool for characterizing the dynamical state of molecular gas in distant galaxies.

We thank the referee for constructive comments. This Letter makes use of the following ALMA data: ADS/JAO. ALMA#2013.1.00742.S. ALMA is a partnership of ESO (representing its member states), NSF (USA) and NINS (Japan), together with NRC (Canada), NSC and ASIAA (Taiwan), and KASI (Republic of Korea), in cooperation with the Republic of Chile. The Joint ALMA Observatory is operated by ESO, AUI/NRAO and NAOJ. K.T. was supported by the ALMA Japan Research Grant of NAOJ Chile Observatory, NAOJ-ALMA-57. This Letter is produced as a part of our collaborations through the joint project supported by JSPS and DAAD under the Japan–German Research Cooperative Program.

References

Barro, G., Kriek, M., Pérez-González, P. G., et al. 2016, ApJL, 827, L32
Barro, G., Trump, J. R., Koo, D. C., et al. 2014, ApJ, 795, 145
Belli, S., Newman, A. B., & Ellis, R. S. 2015, ApJ, 799, 206
Bolatto, A. D., Warren, S. R., Leroy, A. K., et al. 2015, ApJ, 809, 175
Bolatto, A. D., Wolfire, M., & Leroy, A. K. 2013, ARA&A, 51, 207
Bruzual, G., & Charlot, S. 2003, MNRAS, 344, 1000
Burkert, A., Genzel, R., Bouché, N., et al. 2010, ApJ, 725, 2324
Calzetti, D., Armus, L., Bohlin, R. C., et al. 2000, ApJ, 533, 682
Cappellari, M. 2016, ARA&A, 54, 597
Chabrier, G. 2003, PASP, 115, 763
Davies, R., Förster Schreiber, N. M., Cresci, G., et al. 2011, ApJ, 741, 69
Downes, D., & Solomon, P. M. 1998, ApJ, 507, 615
Dunne, L., Eales, S., Ivison, R., Morgan, H., & Edmunds, M. 2003, Natur, 424, 285
Dunne, L., & Eales, S. A. 2001, MNRAS, 327, 697
Fang, J. J., Faber, S. M., Koo, D. C., & Dekel, A. 2013, ApJ, 776, 63
Fontana, A., Dunlop, J. S., Paris, D., et al. 2014, A&A, 570, A11
Galametz, M., Kennicutt, R. C., Albrecht, M., et al. 2012, MNRAS, 425, 763
Hodge, J. A., Swinbank, A. M., Simpson, J. M., et al. 2016, ApJ, 833, 103
Ivison, R. J., Swinbank, A. M., Smail, I., et al. 2013, ApJ, 772, 137
Kriek, M., van Dokkum, P. G., Labbé, I., et al. 2009, ApJ, 700, 221
Law, D. R., Steidel, C. C., Erb, D. K., et al. 2009, ApJ, 697, 2057
Lutz, D., Poglitsch, A., Altieri, B., et al. 2011, A&A, 532, A90
Magrini, L., Bianchi, S., Corbelli, E., et al. 2011, A&A, 535, A13
Martí-Vidal, I., Vlemmings, W. H. T., Muller, S., & Casey, S. 2014, A&A, 563, A136
McMullin, J. P., Waters, B., Schiebel, D., Young, W., & Golap, K. 2007, in ASP Conf. Ser. 376, Astronomical Data Analysis Software and Systems XVI, ed. R. A. Shaw, F. Hill, & D. J. Bell (San Francisco, CA: ASP), 127
Narayanan, D., Krumholz, M. R., Ostriker, E. C., & Hernquist, L. 2012, MNRAS, 421, 3127
Nelson, E., van Dokkum, P., Franx, M., et al. 2014, Natur, 513, 394
Nelson, E. J., van Dokkum, P. G., Momcheva, I. G., et al. 2016, ApJL, 817, L9
Newman, A. B., Belli, S., & Ellis, R. S. 2015, ApJL, 813, L7
Onodera, M., Carollo, C. M., Renzini, A., et al. 2015, ApJ, 808, 161
Popping, G., Decarli, R., Man, A. W. S., et al. 2017, A&A, 602, A11
Sargent, M. T., Daddi, E., Béthermin, M., et al. 2014, ApJ, 793, 19
Scoville, N., Sheth, K., Aussel, H., et al. 2016, ApJ, 820, 83
Skelton, R. E., Whitaker, K. E., Momcheva, I. G., et al. 2014, ApJS, 214, 24
Speagle, J. S., Steinhardt, C. L., Capak, P. L., & Silverman, J. D. 2014, ApJS, 214, 15
Tacchella, S., Carollo, C. M., Forster Schreiber, N. M., et al. 2017, ApJ, submitted (arXiv:1704.00733)
Tacconi, L. J., Genzel, R., Saintonge, A., et al. 2017, ApJ, submitted (arXiv:1702.01140)
Tacconi, L. J., Genzel, R., Smail, I., et al. 2008, ApJ, 680, 246
Tadaki, K.-I., Genzel, R., Kodama, T., et al. 2017, ApJ, 834, 135
Tadaki, K.-I., Kodama, T., Tanaka, I., et al. 2013, ApJ, 778, 114
Tadaki, K.-I., Kohno, K., Kodama, T., et al. 2015, ApJL, 811, L3
van der Wel, A., Chang, Y.-Y., Bell, E. F., et al. 2014, ApJL, 792, L6
van Dokkum, P. G., Bezanson, R., van der Wel, A., et al. 2014, ApJ, 791, 45
Wellons, S., Torrey, P., Ma, C.-P., et al. 2015, MNRAS, 449, 361
Wilson, C. D., Petitpas, G. R., Iono, D., et al. 2008, ApJS, 178, 189
Wisnioski, E., Förster Schreiber, N. M., Wuyts, S., et al. 2015, ApJ, 799, 209
Wuyts, S., Förster Schreiber, N. M., Lutz, D., et al. 2011a, ApJ, 738, 106
Wuyts, S., Förster Schreiber, N. M., van der Wel, A., et al. 2011b, ApJ, 742, 96
Wuyts, S., Förster Schreiber, N. M., Wisnioski, E., et al. 2016, ApJ, 831, 149
Zolotov, A., Dekel, A., Mandelker, N., et al. 2015, MNRAS, 450, 2327